

Exploring a tentative link between FRBs and pulsars with broad energy distributions and applications for nearby FRB survey strategies

S.B. ZHANG,^{1,2} G. HOBBS,² S. JOHNSTON,² S. DAI,² Y. LI,¹ J. S. WANG,³ X. YANG,^{1,4} X. F. WU,^{1,4} AND L. STAVELEY-SMITH^{5,6}

¹*Purple Mountain Observatory, Chinese Academy of Sciences, Nanjing 210023, China*

²*CSIRO Space and Astronomy, Australia Telescope National Facility, PO Box 76, Epping, NSW 1710, Australia*

³*Max-Planck-Institut für Kernphysik, Saupfercheckweg 1, D-69117 Heidelberg, Germany*

⁴*School of Astronomy and Space Sciences, University of Science and Technology of China, Hefei 230026, China*

⁵*International Centre for Radio Astronomy Research, University of Western Australia, Crawley, WA 6009, Australia*

⁶*ARC Centre of Excellence for All Sky Astrophysics in 3 Dimensions (ASTRO 3D)*

ABSTRACT

Fast radio bursts (FRBs) are energetic, short-duration radio pulses of unclear origins. In this study, we investigate the FRBs and pulsars with broad energy distributions by fitting their high energy tails with a power-law model. Two cosmological repeating FRBs (FRB 20201124A and FRB 20220912A), one nearby FRB (FRB 20200120E), and two pulsars (RRATs J1846–0257 and J1854+0306), exhibit power-law indices of $\alpha \gtrsim -1$, suggesting that their bright pulses contribute significantly to the total radio pulse energy. The brightest bursts from these sources fit well with a simple power-law model ($\alpha = -0.26 \pm 0.05$), indicating a tentative link between certain high-luminosity FRBs and low-luminosity radio bursts. We also discuss detailed survey strategies for FAST, MeerKAT and Parkes cryoPAF in the search for FRBs in nearby globular clusters (GCs) using different power-law indices, recommending targets for observation. We suggest that combining observations with FAST (~ 3 hours) and Parkes cryoPAF (10–20 hours) are practicable for discovering new FRBs in the nearby GCs.

Keywords: Radio bursts (1339), Radio transient sources (2008), Radio pulsars (1353)

1. INTRODUCTION

Fast radio bursts (FRBs) are immensely energetic radio pulses with durations ranging from microseconds to seconds (Lorimer et al. 2007; Snelders et al. 2023; Chime/Frb Collaboration et al. 2022). Among the nearly one thousand known FRB sources, fewer than 10% exhibit repeat bursts (CHIME/FRB Collaboration et al. 2021; Spitler et al. 2016; Chime/Frb Collaboration et al. 2023). The origin of FRBs remains unclear, but the only two nearby events offer clues to their engines: the apparently one-off burst FRB 20200428 from the Galactic magnetar SGR 1935+2154 (Bochenek et al. 2020; CHIME/FRB Collaboration et al. 2020) and the repeating FRB 20200120E, localized to a globular cluster (GC) in the M81 galactic system at a distance of 3.63 Mpc (Bhardwaj et al. 2021; Kirsten et al. 2022). While these two events suggest connections to distinct environments, young magnetars and ancient star populations, respectively, both have propelled FRB theories involving compact objects, especially neutron stars, as potential sources (Zhang 2023).

The typical energy of cosmological repeating FRBs (Li et al. 2021; Xu et al. 2022; Chime/Frb Collaboration et al. 2020) is approximately four orders of magnitude greater than that of the two nearby FRBs (Bochenek et al. 2020; Nimmo et al. 2023), and about twelve orders of magnitude larger than that of pulsars¹ (Manchester et al. 2005). However, the detection of a bright burst from FRB 20200120E (Zhang et al. 2024a) bridges the gap between nearby and cosmological FRBs. Similarly, the detection of radio bursts with varying luminosities from SGR 1935+2154 (Bochenek et al. 2020; CHIME/FRB Collaboration et al. 2020; Kirsten et al. 2021; Good & Chime/Frb Collaboration 2020; Zhu et al. 2023) connects the energy range of nearby FRBs to that of pulsars. As presented in Figure 1 of Zhang et al. (2024a), no clear gap exists between the estimated isotropic-equivalent energy releases of various radio pulses.

¹ <http://www.atnf.csiro.au/research/pulsar/psrcat>

It is intriguing to explore whether nearby radio pulse phenomena can be connected to cosmological FRBs, particularly repeating ones. Follow-up observation of repeating FRBs (Li et al. 2021; Xu et al. 2022; Zhang et al. 2023) have revealed extremely variable properties, especially in energy, spanning more than three orders of magnitude. In contrast, broad energy distributions are atypically for single pulses from pulsars (Burke-Spolaor et al. 2012). Intensity variations exceeding an order of magnitude are usually attributed to the rare phenomenon of “giant pulses” (Kuzmin 2007), reported in only about ten (Wang et al. 2019) of the more than 3500 known pulsars (Manchester et al. 2005). However, recent observations of some of another kind of special pulsars (Zhang et al. 2024b; Zhang et al. 2024), rotating radio transients (RRATs), characterized by sporadic radio pulses, have also shown broad energy distributions. It is still worthy to explore the potential relation between FRBs and these pulsars with broad energy distributions.

A few hyperactive repeating FRBs provide large samples of $\gtrsim 1000$ burst, enabling detailed studies of their energy distributions (Li et al. 2021; Xu et al. 2022; Zhang et al. 2023). Notably, two such sources—FRB 20201124A and FRB 20220912A—have been observed for more than 2000 hours, revealing breaks in their burst energy distributions, with a flattening of the power-law slope ($\gtrsim -1$) at higher energies (Kirsten et al. 2024; Ould-Boukattine et al. 2024). It is also noteworthy that the detection of a bright burst from the nearby FRB 20200120E indicates a similar flat energy distribution, with a power-law index of approximately -0.98 (Zhang et al. 2024a). Furthermore, two RRATs have also exhibited power-law-like tails at high energies with similarly flat indices (Zhang et al. 2024). These observations suggest that flat power-law tails at high energies may offer a clue into the mechanisms underlying these short-duration radio pulses with diverse energy releases.

In this study, we present an analysis of the energy distributions tails at high energy of FRBs and pulsars using a consistent method. Section 2 describes the sources selection and data processing, while Section 3 and 4 presents and discusses the results. We conclude in Section 5.

2. SOURCES SELECTION AND DATA PROCESSING

2.1. Sources selection

The selected sources, presented in Figure 1, show the brightest strong pulses that are at least 2–3 orders of magnitude more energetic than their relatively weak emissions. The energies of the detected radio pulses from these sources span roughly 15 orders of magni-

tude. Specifically, the studied sources include: (1) FRB 20201124A and FRB 20220912A: These are the only two FRBs with up to 2000 hours of follow-up observations, during which ultra-luminous bursts with isotropic energy up to 10^{41} erg were detected (Kirsten et al. 2024; Ould-Boukattine et al. 2024), placing them among the most energetic FRBs observed. (2) FRB 20200120E: A nearby FRB that exhibited a burst storm (Nimmo et al. 2023) and an abnormal burst more than 42 times brighter than previously detected bursts at a similar frequency (Zhang et al. 2024a). (3) J0534+2200 (the Crab pulsar) and J0540–6919: These pulsars are known for producing giant pulses with the largest excesses relative to their normal emissions (Bera & Challengar 2019; Geyer et al. 2021; Wang et al. 2019). (4) RRATs J1846–0257 and J1854+0306: These RRATs have relatively high surface magnetic fields ($\sim 2 \times 10^{13}$ G) and show weak emissions that are up to 687 and 512 times fainter than their strong individual pulses. We also analysed data from RRAT J1913+1330 (Zhang et al. 2024b), which exhibits extreme pulse-to-pulse modulation and an energy distribution spanning 3 orders of magnitude but could be well-fitted by two log-normal functions. Its distribution tail at the high energy part provides a useful comparison with the four source kinds above.

2.2. Data processing

To compare the energy distributions of different radio pulses, we calculated the specific isotropic-equivalent energy using (Zhang 2018):

$$E_S = \frac{4\pi D_L^2}{1+z} F, \quad (1)$$

where D_L is the luminosity distance, z is the redshift, and F is the pulse fluence. The energy values for each source were then normalized to their brightest bursts.

Since only one bright burst has been detected from FRB 20200120E (Zhang et al. 2024a) and detailed burst properties for FRB 20220912A are currently unavailable (Ould-Boukattine et al. 2024), we were unable to reprocess their high-energy distributions. To compare our results with their reported distributions, which are cumulative, our initial analysis used a cumulative distribution, adjusting the bins for each source to cover a similar range in log-10 space. We also provide a differential distribution analysis. To enable comparisons between different sources, we defined a density that is calculated as the number of bursts per bin divided by the total number of detected bursts.

The power-law-like tails were fitted using the Python package CURVE_FIT function from the SCIPY li-

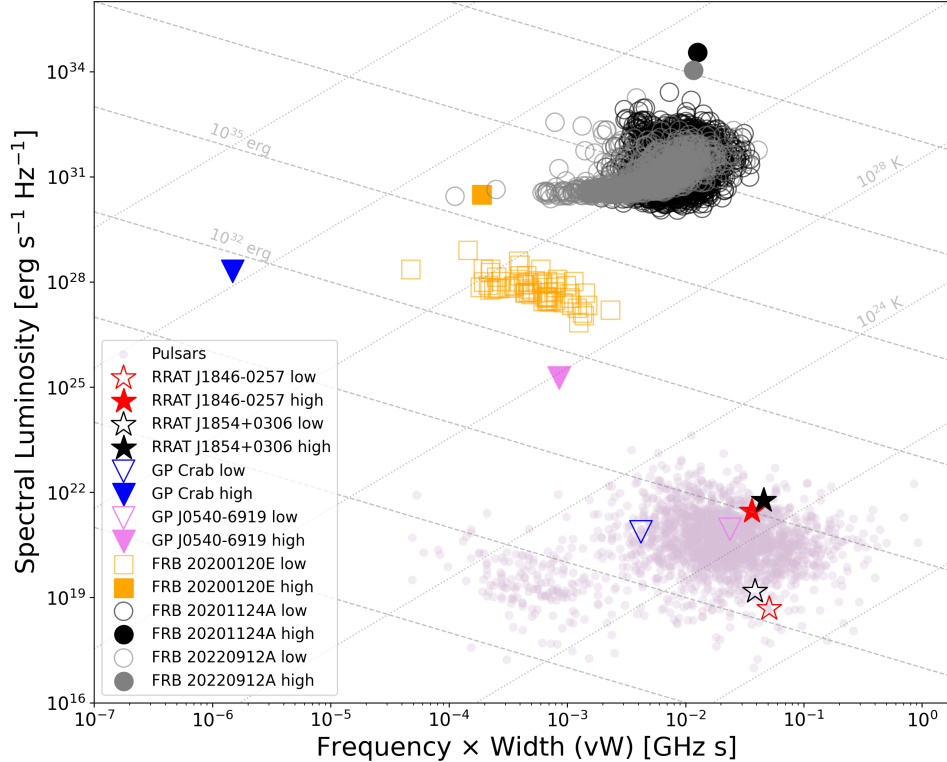


Figure 1. Isotropic-equivalent spectral luminosity versus the product of observing frequency and pulse width for various pulsars and FRBs. The brightest strong pulses from RRATs with relatively high B_s (J1846-0257 and 1854+0306) are represented by red and black filled stars, while their weak emissions are denoted by unfilled stars (Zhang et al. 2024). The brightest giant pulses from J0534+2200 (Crab pulsar) (Bera & Chengalur 2019) and J0540–6919 (Geyer et al. 2021) are shown as blue and violet filled triangles, with their normal emissions (Manchester et al. 2005) marked by unfilled triangles. The brightest burst from the nearby FRB 20200120E (Zhang et al. 2024a) is indicated by an orange filled square, with its relatively weaker bursts (Nimmo et al. 2023) are marked by unfilled squares. The brightest bursts from cosmological FRB 20201124A (Kirsten et al. 2024) and FRB 20220912A (Ould-Boukattine et al. 2024) are represented by black and gray filled circles, with their relatively weaker bursts (Xu et al. 2022; Zhang et al. 2023) shown as unfilled circles. The pulsar (Manchester et al. 2005) population is indicated in thistle. Grey dashed lines represent constant isotropic-equivalent energy release, while grey dotted lines indicate constant brightness temperature.

brary (Virtanen et al. 2020). For data with complex uncertainties, we performed the fitting within a Bayesian framework using Markov Chain Monte Carlo (MCMC) sampling, via the EMCEE Python package (Foreman-Mackey et al. 2013).

3. RESULTS

Figure 2 presents the cumulative specific energy distributions of high-energy bursts from the selected sources with relatively sufficient burst counts, most of which can be well-fitted by a simple power-law model. The high-energy tail of the distribution for RRAT J1913+1330 is forcefully fitted using a power-law function, although the fit is not as good as for the other sources, in order to enable comparison. Specifically, the fitted

power-law indices (α) for FRB 20201124A (46 bursts ²), RRATs J1846–0257 (72 bright pulses) and J1854+0306 (325 bright pulses) are -0.75 ± 0.14 , -0.84 ± 0.10 and -0.76 ± 0.03 , respectively, all of which are $\gtrsim -1$. In contrast, the indices for the Crab pulsar (-1.98 ± 0.07 , 1955 giant pulses), J0540–6919 (-2.29 ± 0.07 , 865 bright single pulses) and RRAT J1913+1330 (-3.04 ± 0.29 , 1955 individual pulses) are significantly steeper, at $\lesssim -2$. Although the available data for bursts from FRB 20200120E and FRB 20220912A are insufficient to re-process their high-energy distributions, the reported fitted power-law indices are -0.98 ± 0.06 (Zhang et al. 2024a) for FRB 20200120E and range from -0.99 to -0.60 (Ould-Boukattine et al. 2024) for FRB 20220912A at around 1.4 GHz, both indicate relatively flat indices.

² For events detected simultaneously by multiple telescopes, we selected bursts from the observation with the largest bandwidth.

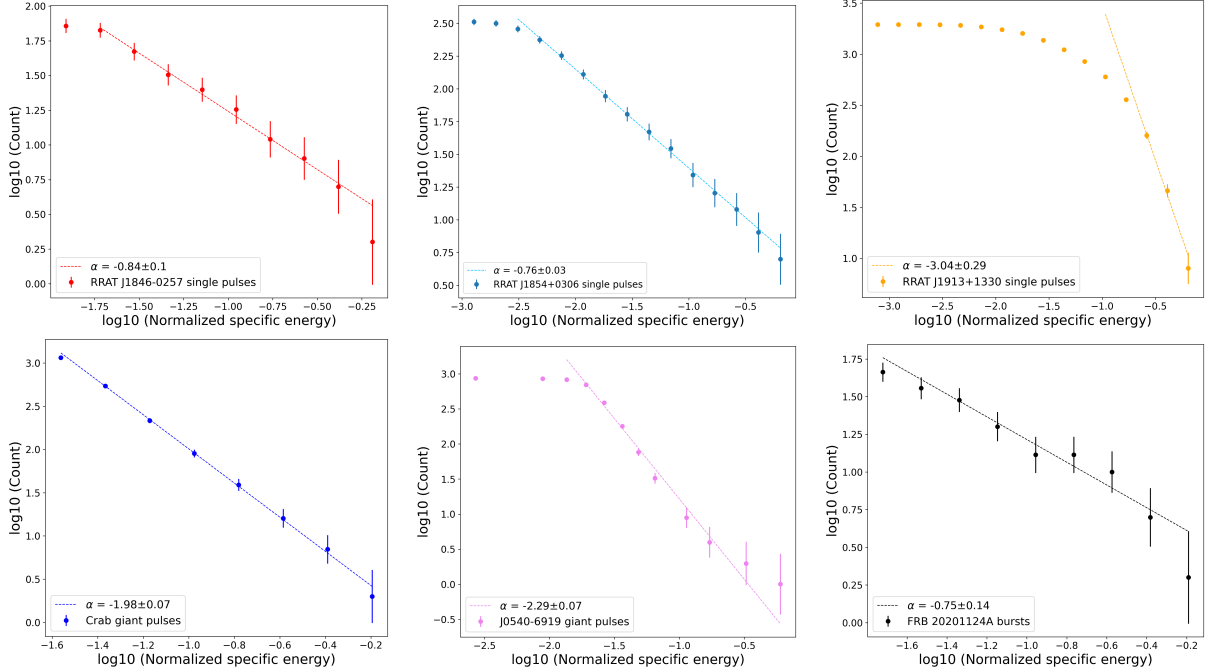


Figure 2. Cumulative specific energy distributions of high-energy bursts from FRB 20201124A, single pulses from RRATs J1913+1330, J1846–0257, and J1854+0306, and giant pulses from the Crab pulsar (J0534+2200) and J0540–6919. The energy values for each source are normalized to their respective brightest bursts. Each high-energy tail is fitted with a simple power law model.

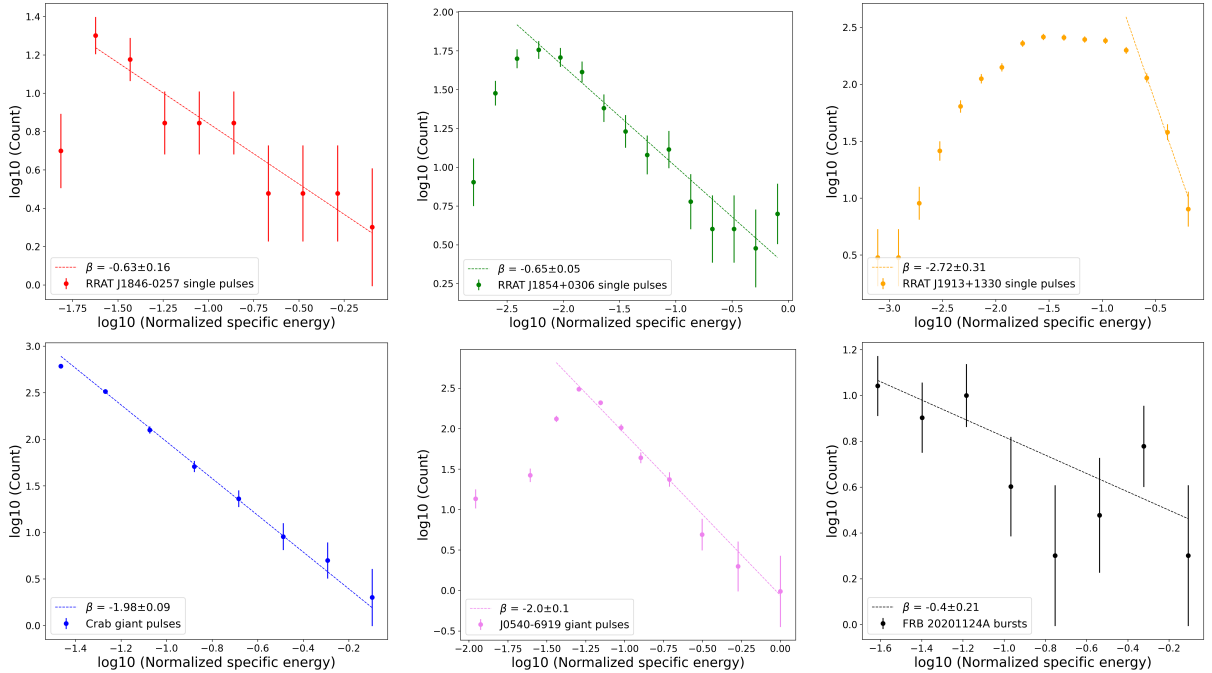


Figure 3. Differential specific energy distributions of high-energy bursts from FRB 20201124A, single pulses from RRATs J1913+1330, J1846–0257, and J1854+0306, and giant pulses from the Crab pulsar (J0534+2200) and J0540–6919. The energy values for each source are normalized to their respective brightest bursts. Each high-energy tail is fitted with a simple power law model.

Furthermore, we also present the differential specific energy distributions of high-energy bursts from these

source in Figure 3. Similar to the cumulative distributions, the fitted indices using a power-law func-

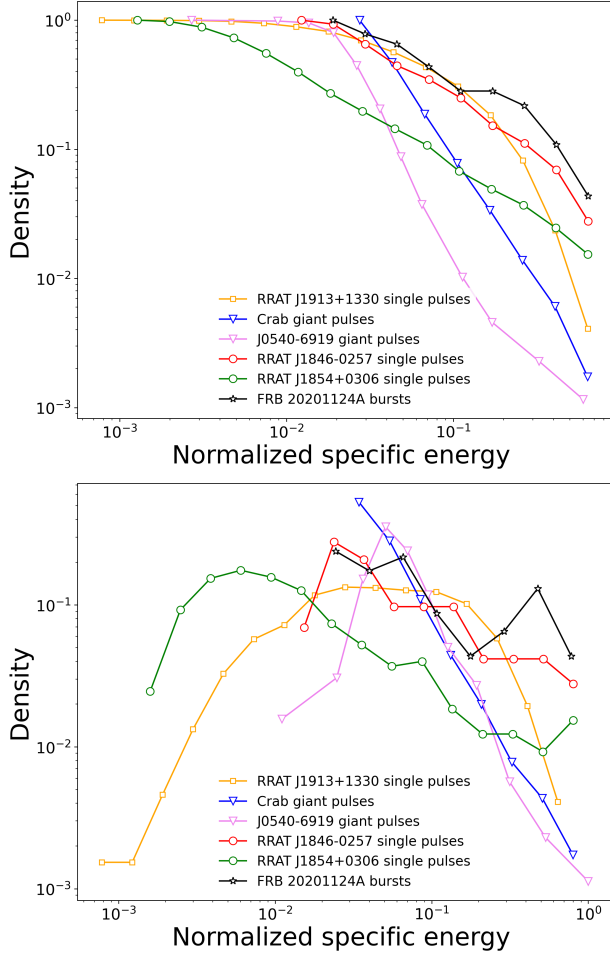


Figure 4. Comparison of cumulative (top) and differential (bottom) normalized specific energy distributions of high-energy bursts from FRB 20201124A, single pulses from RRATs J1913+1330, J1846–0257, and J1854+0306, and giant pulses from the Crab pulsar (J0534+2200) and J0540–6919. The energy values for each source are normalized to their respective brightest bursts. The density represents the number of bursts per bin divided by the total number of detected bursts.

tion for the differential distributions at the high energy tails (β) of FRB 20201124A (-0.40 ± 0.21), RRATs J1846–0257 (-0.63 ± 0.16) and J1854+0306 (-0.65 ± 0.05) are significantly flatter than those of the Crab pulsar (-1.98 ± 0.09), J0540–6919 (-2.0 ± 0.1) and RRAT J1913+1330 (-2.72 ± 0.31). However, the sample sizes for some sources, especially RRAT J1846–0257 and FRB 20201124A, are limited, and the fitted uncertainties are relatively large.

As shown in the comparison in Figure 4, the energy distributions of FRB 20201124A, RRATs J1846–0257 and J1854+0306 decline much more slowly at high energies compared to those of the giant-pulse pulsars and RRAT J1913+1330.

4. DISCUSSION

4.1. Bright bursts of various radio sources

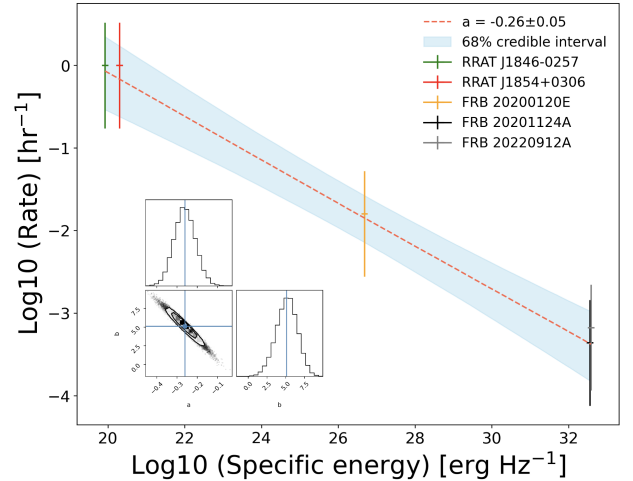


Figure 5. Specific energy of the brightest bursts versus their detection rates for FRB 20201124A, FRB 20220912A, FRB 20200120E and the RRATs J1846–0257 and J1854+0306. The data are fitted with a power law relation (red dashed line) using a Bayesian framework, and the shaded region represents the 68% credible interval for the fit. Posterior distributions and a parameter correlation plot for the power law fit parameters are shown in the inset.

Sources with flat energy distributions ($\alpha \gtrsim -1$) at high energies suggest that their “bright pulses” might contribute significantly to the total pulse energy release. Therefore, the detection of the brightest bursts from these sources could provide insight into a potential connection between cosmological high-luminosity radio bursts and nearby low-luminosity ones. Figure 5 presents the specific energy of the brightest bursts and the corresponding detection rates for the studied sources with flat energy distributions, i.e., RRATs J1846–0257 and J1854+0306, FRB 20200120E, FRB 20201124A and FRB 20220912A. Interestingly, these data points align well with a simple power-law fit of $\alpha = -0.26 \pm 0.05$. Due to the sample size of only five points and the stochastic nature of detecting the “brightest burst”, we remain cautious about interpreting this correlation as a physical relationship. Nevertheless, this trend suggests that high-luminosity radio bursts, such as FRBs, could be naturally derived from low-luminosity radio bursts, such as those from pulsars. Although an extremely shallow power-law index is implied, the flatter energy distributions at higher energies observed in these sources may provide clues for understanding this tentative connection.

4.2. Survey strategies for nearby FRBs

As presented in Figure 2 and 3 of Section 3, the fitting of the cumulative energy distribution at high energies using a power-law function yields better results with smaller uncertainties compared to the differential distributions. This difference may arise because the limited burst numbers for the studied sources are insufficient to provide a reliable sample for the differential distributions. Therefore, we used the power-law indices (α) derived from the cumulative energy distribution to estimate the detection rate in this section, which is given by:

$$\log_{10}N(\geq E) = C + \alpha \log_{10}E, \quad (2)$$

where $N(\geq E)$ represents the predicted number of bursts with specific energy above E .

For a telescope operating at a fluence completeness threshold of F_{det} , bursts with energy above the threshold $E_{\text{det}} = 4\pi D_{\text{det}}^2 F_{\text{det}}$ are expected to be detected, where D_{det} is the distance to the target source, and assuming a detected burst rate of R_{det} . Applying Equation 2, the burst rate expected for bursts detectable by an arbitrary radio telescope with a fluence threshold F_{th} , for a source at a distance of D_{tar} , can be written as:

$$R_{\text{th}} \approx R_{\text{det}} \times \left(\frac{F_{\text{th}}}{F_{\text{det}}}\right)^\alpha \left(\frac{D_{\text{tar}}}{D_{\text{det}}}\right)^{2\alpha}. \quad (3)$$

Kremer et al. (2023) presented prospects for detecting FRBs from GC in nearby galaxies using FAST (Jiang et al. 2020) and MeerKAT (Bailes et al. 2020), suggesting that NGC 4486 (M87) could be the best candidate target. However, the fluence threshold (F_{th}) of a telescope may be significantly affected by the continuum radio flux densities (S_{tar}) from the target galaxies (Suresh et al. 2021), which was not thoroughly discussed in detection rate estimation by Kremer et al. (2023). Taking into account S_{tar} and the telescope's corresponding system-equivalent flux density (SEFD), the radiometer equation (Lorimer & Kramer 2004) for estimating the minimum detectable fluence can be written as:

$$F_{\text{min}} = \frac{S/N_{\text{min}}(\text{SEFD} + S_{\text{tar}})}{\sqrt{\Delta\nu N_p W}} \times W, \quad (4)$$

where we ignore the loss factor, $S/N_{\text{min}} \sim 7$ is the signal-to-noise ratio (S/N) threshold typically applied in the single-pulse search pipeline, $\Delta\nu$ is the bandwidth, N_p is the number of polarization, and W is the burst width³. The FAST telescope has a system temperature of ~ 20 K and a gain of 16K/Jy (Jiang et al. 2020), resulting in a corresponding SEFD of $S_{\text{FAST}} = 1.25$ Jy, while

³ In this study, we used $W \sim 1$ ms to estimate the sensitivity.

MeerKAT has a system temperature of ~ 18 K and a gain of 2.8K/Jy (Bailes et al. 2020), resulting in a corresponding SEFD of $S_{\text{MeerKAT}} = 6.43$ Jy. The galaxy M87 could contribute S_{tar} up to 210 Jy at 1.4 GHz (Brown et al. 2011), meaning the effective detectable fluence of sources in M87 for FAST and MeerKAT would be approximately 169 and 34 times larger, respectively. Therefore, for telescopes with high sensitivities, galaxies with relatively small S_{tar} , such as NGC 4649 (M60), which has $S_{\text{tar}} \sim 0.03$ at 1.4 GHz (Brown et al. 2011) and is estimated to contain approximately 4000 GCs (Harris et al. 2013), could be more efficient search targets.

At a given distance, the number of potential sources is proportional to the field of view (FOV) of the telescope. Combining the FOV with Equation 3, the detection rate of the telescope is given by:

$$R \propto F_{\text{th}}^\alpha \cdot D_{\text{tar}}^{2\alpha} \cdot \text{FOV}. \quad (5)$$

For smaller values of α , the telescope's sensitivity dominates the detection rate, whereas for larger values of α the FOV becomes more important. Therefore, in addition to telescopes with high sensitivity, such as FAST and MeerKAT, observations with large FOV but relatively lower sensitivity may also be efficient for capturing such events.

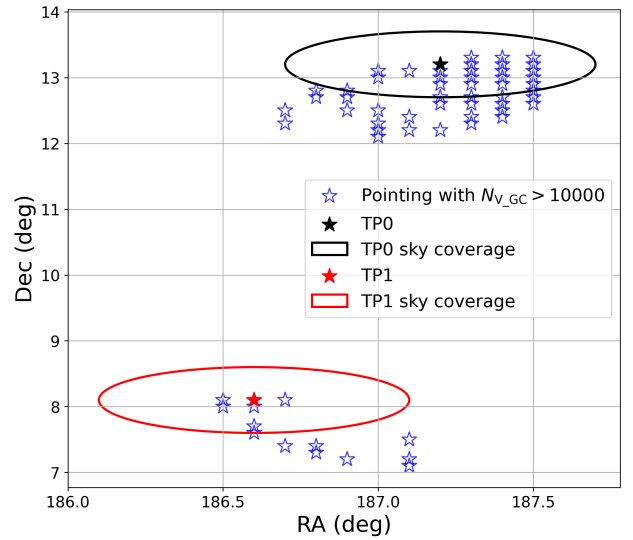


Figure 6. Parkes cryoPAF 63 pointings covering more than 10,000 valid GCs. The two most suggested pointings, TP0 (Dec ~ 13 deg) and TP1 (Dec ~ 8 deg), are marked by black and red stars, respectively, with their corresponding sky coverage shown by circles.

A cryogenic phased array receiver (cryoPAF) is currently being completed and tested on the Parkes telescope. The new cryoPAF is expected to have a system

Table 1. Properties of the 24 GC systems covered by Parkes cryoPAF pointing TP0 (RA = 187.2 deg; Dec = 13.2 deg). d_L and D_{TP} represent the distance from the GC system centre to the earth and the pointing, respectively. References for the galaxy continuum radio flux densities at 1.4 GHz ($S_{\text{tar},1.4\text{GHz}}$) are: (a) Brown et al. (2011), (b) Allison et al. (2014), (c) estimated from National Radio Astronomy Observatory Very Large Array Sky Survey (NVSS, <https://www.cv.nrao.edu/nvss/>), (d) Nyland et al. (2017), (e) Oosterloo et al. (2010).

Name	RA (deg)	Dec (deg)	d_L (Mpc)	D_{TP} (deg)	N_{GC}	N_{V_GC}	$S_{\text{tar},1.4\text{GHz}}$ (Jy)
NGC4486 (M87)	187.706	12.391	17.0	0.95	13000	6500	~ 210 (a)
NGC4374 (M84)	186.265	12.887	18.5	0.96	4301	4301	~ 6.1 (b)
NGC4406 (M86)	186.549	12.946	17.1	0.68	2800	2800	< 0.1 (c)
NGC4473	187.454	13.429	15.2	0.34	376	376	< 0.1 (a)
NGC4435	186.919	13.079	16.6	0.30	345	345	< 0.1 (c)
NGC4459	187.250	13.979	16.0	0.78	218	218	< 0.1 (d)
NGC4474	187.473	14.069	15.5	0.91	116	116	< 0.1 (c)
NGC4458	187.240	13.242	16.3	0.06	72	72	< 0.1 (e)
NGC4387	186.424	12.810	18.0	0.85	70	70	< 0.1 (e)
VCC-940	186.696	12.454	18.7	0.89	61	61	< 0.1 (c)
NGC4479	187.577	13.578	17.4	0.53	59	59	< 0.1 (c)
NGC4478	187.574	12.327	17.0	0.95	58	58	< 0.1 (c)
VCC-1386	187.964	12.657	16.0	0.92	27	27	< 0.1 (c)
NGC4476	187.496	12.349	17.7	0.90	20	20	< 0.1 (c)
VCC-871	186.523	12.560	16.0	0.92	18	18	< 0.1 (c)
VCC-965	186.763	12.561	16.9	0.77	15	15	< 0.1 (c)
VCC-1185	187.348	12.451	16.9	0.76	14	14	< 0.1 (c)
NGC4431	186.864	12.290	15.8	0.97	11	11	< 0.1 (c)
VCC-1104	187.117	12.824	15.7	0.38	8	8	< 0.1 (c)
VCC-896	186.594	12.787	16.0	0.72	5	5	< 0.1 (c)
VCC-1105	187.114	14.156	16.0	0.96	5	5	< 0.1 (c)
NGC4486B	187.633	12.490	16.3	0.83	4	4	~ 0.4 (c)
VCC-1272	187.567	13.308	16.0	0.37	3	3	< 0.1 (c)
VCC-1077	187.043	12.807	16.0	0.42	2	2	< 0.1 (c)

Table 2. Properties of the 12 GC systems covered by Parkes cryoPAF pointing TP1 (RA = 186.6 deg; Dec = 8.1 deg). d_L and D_{TP} represent the distance from the GC system centre to the earth and the pointing, respectively. References for the galaxy continuum radio flux densities at 1.4 GHz ($S_{\text{tar},1.4\text{GHz}}$) are: (a) White & Becker (1992), (b) Brown et al. (2011), (c) estimated from National Radio Astronomy Observatory Very Large Array Sky Survey (NVSS, <https://www.cv.nrao.edu/nvss/>).

Name	RA (deg)	Dec (deg)	d_L (Mpc)	D_{TP} (deg)	N_{GC}	N_{V_GC}	$S_{\text{tar},1.4\text{GHz}}$ (Jy)
NGC4472 (M49)	187.445	8.000	17.0	0.84	7000	7000	~ 0.8 (a)
NGC4365	186.118	7.318	23.3	0.92	3246	3246	< 0.1 (b)
NGC4434	186.903	8.154	22.5	0.30	141	141	< 0.1 (c)
VCC-1254	187.521	8.074	16.0	0.91	26	26	< 0.1 (c)
VCC-1107	187.126	7.325	16.0	0.93	25	25	< 0.1 (c)
NGC4464	187.339	8.157	15.8	0.73	25	25	< 0.1 (c)
NGC4318	185.680	8.198	22.1	0.92	18	18	< 0.1 (c)
VCC-747	186.199	8.992	18.5	0.98	16	16	< 0.1 (c)
VCC-1167	187.301	7.879	16.0	0.73	14	14	< 0.1 (c)
VCC-571	185.671	7.950	23.8	0.93	11	11	< 0.1 (c)
VCC-1049	186.978	8.090	16.0	0.37	8	8	< 0.1 (c)
VCC-992	186.828	8.213	16.0	0.25	4	4	< 0.1 (c)

temperature of < 20 K and a gain of 0.735K/Jy, resulting in a corresponding SEFD of $S_{\text{Parkes}} = 27.21$ Jy. Its wide FOV spans up to 3 square degrees and consists of

72 adjacent beams, covering a frequency range of 700-

1950 MHz⁴. Based on the cryoPAF’s sky coverage, which is modelled as a circle with a radius of approximately 1 deg in this work, and the catalogue of GC systems (Harris et al. 2013) within a relatively close distance (< 40 Mpc), we conducted a grid analysis of the sky with a 0.1 deg step size to estimate the number of GCs covered by the cryoPAF FOV. Notably, about 20% of GCs lie within a 4-arcminute radius of the centre of M87 (Strader et al. 2011), where the radio background is comparable to S_{Parkes} (Perley & Butler 2017). Given this, the cryoPAF observation should cover the majority of GCs in M87 with adequate sensitivity, and we adopt a conservative estimate that 50% of the GCs are valid targets for Parkes observation (denoted as N_{V_GC}). As shown in Figure 6, among the more than 6,000,000 analysed pointings, 63 could cover more than 10,000 valid GCs, all with Dec near 13 or 8 deg. Pointings TP0 (RA = 187.2 deg; Dec = 13.2 deg) and TP1 (RA = 186.6 deg; Dec = 8.1 deg) cover the largest number of valid GCs in these two Dec ranges. Based on this, we suggest these two pointings as the best targets for searching for FRBs in nearby GCs. As listed in Tables 4.2 and 4.2, the Parkes cryoPAF pointing TP0 could cover 24 GC systems, expected to include 21,607 GCs, of which 15,107 are valid targets. TP1 could cover 12 GC systems, expected to include 10,535 GCs, all of which are valid.

Furthermore, we estimated the predicted FRB detection rates for FAST and MeerKAT targeting M60, as well as for Parkes cryoPAF targeting TP0 and TP1, using power-law indices $\alpha = -0.2, -0.5, -1.0, -1.5$ and -2.0 . Most of the essential values used in this calculation are similar to Kremer et al. (2023). The fluence thresholds of FAST and MeerKAT are 0.015 Jy ms (Niu et al. 2021) and 0.09 Jy ms (Bailes et al. 2020). The reference values for the detection rate ($R_{\text{det}} \sim 0.07 \text{ hr}^{-1}$), fluence threshold ($F_{\text{det}} \sim 5 \text{ Jy ms}$), and source distance ($D_{\text{det}} \sim 3.63 \text{ Mpc}$) were derived from CHIME’s observations of FRB 20200120E (CHIME/FRB Collaboration et al. 2021; Bhardwaj et al. 2021; Kirsten et al. 2022). The detection of a single FRB repeater by CHIME in the GCs within the M81 region suggests a specific abundance of $N_{\text{obs}} \sim 1/900 \approx 1.1 \times 10^{-3}$ (Bhardwaj et al. 2021; Harris et al. 2013; Kremer et al. 2023), with a 90% confidence range of $(5.6 \times 10^{-3}, 3.3 \times 10^{-3})$, incorporating the Poisson probability (Lu et al. 2022). For GC

systems with $S_{\text{tar},1.4\text{GHz}} < 0.1 \text{ Jy}$, which are negligible compared to the SEFDs of all three telescopes, we ignored their effect on the minimum detectable fluence. For GCs with larger $S_{\text{tar},1.4\text{GHz}}$, we used the effective minimum detectable fluence calculated using by Equation 4.

As presented in Table 4.2, for steep power-law indices ($\alpha = -1.5, -2.0$), FAST is the most powerful telescope for detecting nearby FRBs, with a detection rate of up to 20 hr^{-1} . Even at the lower detection rate limits, only about 3 hours of observation are required to expect a new detection. In contrast, Parkes cryoPAF is more efficient for flatter indices ($\alpha = -0.2, -0.5, -1.5$), with 10 to 20 hours of observation typically required to ensure detecting a new source.

5. CONCLUSION

Before the discovery of a population of FRBs (Thornton et al. 2013) that supported the astrophysical origin of the ‘‘Lorimer burst’’ (Lorimer et al. 2007), pulsars (Manchester et al. 2005) were considered the primary sources of bright, short-duration (\lesssim second) radio pulses, which require coherent emission (Pietka et al. 2015). While FRBs also necessitate coherent emission, their luminosities are more than ten orders of magnitude higher. Initially, the apparent one-off nature of FRBs led to favouring catastrophic scenarios (Zhang 2023), distinguishing them from pulsars. However, the discovery of repeating FRBs (Spitler et al. 2016), and the investigation that some Galactic radio pulsing sources might be one-off (Keane 2016; Zhang & Yang 2024), have reduced this distinction. Further observations of fainter FRB bursts (Bochenek et al. 2020; CHIME/FRB Collaboration et al. 2020; Nimmo et al. 2023; Zhang et al. 2024a) and brighter pulses from magnetars or pulsars (Kirsten et al. 2021; Good & Chime/Frb Collaboration 2020; Bera & Chengalur 2019) suggest no clear gap between the isotropic-equivalent energy releases of various radio pulses (Zhang et al. 2024a). Additionally, polarimetric similarities between FRBs and pulsars have been observed (Feng et al. 2022; Niu et al. 2024). These findings highlight the importance of exploring potential connections between FRBs and pulsars, at least for certain sources.

In this study, we have presented similarities in the high-energy distributions of two cosmological repeating FRBs (FRB 20201124A and FRB 20220912A), one nearby FRB 20200120E, and two pulsars (RRATs J1846–0257 and J1854+0306). All these sources exhibit power-law indices of $\alpha \gtrsim -1$, suggesting that their ‘‘bright pulses’’ might significantly contribute to the total radio pulse energy release. Furthermore, the

⁴ As cryoPAF is still being tested, the accurate parameters of the full-beam system performance are unavailable for now. We used the values referenced from the Parkes cryoPAF introduction by Alex Dunning: https://research.csiro.au/ratechnologies/wp-content/uploads/sites/295/2022/11/PAFAR2022-Dunning-CryoPAF_for_Parkes.pdf

Table 3. Predicted FRB detection rates in nearby GC systems by FAST, MeerKAT and Parkes cryoPAF.

Target	Instrument	N_{GC}	N_{V_GC}	FRB detection rate (hr^{-1})				
				$\alpha = -0.2$	$\alpha = -0.5$	$\alpha = -1.0$	$\alpha = -1.5$	$\alpha = -2.0$
M60	FAST	4000	1203	0.16(0.01–0.48)	0.35(0.02–1.06)	1.36(0.07–4.08)	5.21(0.27–15.64)	19.98(1.02–59.93)
M60	MeerKAT	4000	4000	0.37(0.02–1.11)	0.49(0.02–1.46)	0.77(0.04–2.31)	1.21(0.06–3.64)	1.92(0.1–5.75)
TP0	Parkes cryoPAF	21607	15107	1.3(0.07–3.89)	1.53(0.08–4.6)	2.03(0.1–6.1)	2.72(0.14–8.15)	3.65(0.19–10.96)
TP1	Parkes cryoPAF	10535	10535	0.88(0.04–2.65)	1.01(0.05–3.03)	1.28(0.07–3.84)	1.65(0.08–4.94)	2.15(0.11–6.44)

brightest bursts from these sources fit well with a simple power-law model of $\alpha = -0.26 \pm 0.05$. However, considering the limited sample size, we advise caution in interpreting this correlation as physical.

We encourage further observations to expand the sample of high-energy bursts from both FRB-like and pulsar-like sources. Current FRB surveys may be limited by selection effects, potentially missing FRBs with relative low-luminosity from the nearby GC systems (Zhang et al. 2024a). Survey strategies will need to vary for sources with different energy distributions. In this work, we have discussed detailed survey strategies for FAST, MeerKAT and Parkes cryoPAF for FRB in nearby GCs and suggested optimal survey targets. In principle, conducting combining observations for these targets using FAST for about 3 hours and Parkes cryoPAF for 10 – 20 hours could potentially lead to the discovery of new FRBs in nearby GCs, in practice. Additionally, a lack of detection after even a few hours of FAST observation can still provide strict constraints on flat α values.

ACKNOWLEDGMENTS

This research has been partially funded by the National SKA Program of China (2022SKA0130100), the National Natural Science Foundation of China (grant Nos. 12041306,12273113,12233002,12003028,12321003), the CAS Project for Young Scientists in Basic Research (Grant No. YSBR-063), the International Partnership Program of Chinese Academy of Sciences for Grand Challenges (114332KYSB20210018), the ACA-MAR Postdoctoral Fellow, China Postdoctoral Science Foundation (grant No. 2020M681758), and the Natural Science Foundation of Jiangsu Province (grant Nos. BK20210998).

- Allison, J. R., Sadler, E. M., & Meekin, A. M. 2014, *MNRAS*, 440, 696, doi: [10.1093/mnras/stu289](https://doi.org/10.1093/mnras/stu289)
- Bailes, M., Jameson, A., Abbate, F., et al. 2020, *PASA*, 37, e028, doi: [10.1017/pasa.2020.19](https://doi.org/10.1017/pasa.2020.19)
- Bera, A., & Chengalur, J. N. 2019, *MNRAS*, 490, L12, doi: [10.1093/mnrasl/slz140](https://doi.org/10.1093/mnrasl/slz140)
- Bhardwaj, M., Gaensler, B. M., Kaspi, V. M., et al. 2021, *ApJL*, 910, L18, doi: [10.3847/2041-8213/abeaa6](https://doi.org/10.3847/2041-8213/abeaa6)
- Bochenek, C. D., Ravi, V., Belov, K. V., et al. 2020, *Nature*, 587, 59, doi: [10.1038/s41586-020-2872-x](https://doi.org/10.1038/s41586-020-2872-x)
- Brown, M. J. I., Jannuzi, B. T., Floyd, D. J. E., & Mould, J. R. 2011, *ApJL*, 731, L41, doi: [10.1088/2041-8205/731/2/L41](https://doi.org/10.1088/2041-8205/731/2/L41)
- Burke-Spolaor, S., Johnston, S., Bailes, M., et al. 2012, *MNRAS*, 423, 1351, doi: [10.1111/j.1365-2966.2012.20998.x](https://doi.org/10.1111/j.1365-2966.2012.20998.x)
- CHIME/FRB Collaboration, Andersen, B. C., Bandura, K. M., et al. 2020, *Nature*, 587, 54, doi: [10.1038/s41586-020-2863-y](https://doi.org/10.1038/s41586-020-2863-y)
- Chime/Frb Collaboration, Amiri, M., Andersen, B. C., et al. 2020, *Nature*, 582, 351, doi: [10.1038/s41586-020-2398-2](https://doi.org/10.1038/s41586-020-2398-2)
- CHIME/FRB Collaboration, Amiri, M., Andersen, B. C., et al. 2021, *ApJS*, 257, 59, doi: [10.3847/1538-4365/ac33ab](https://doi.org/10.3847/1538-4365/ac33ab)
- Chime/Frb Collaboration, Andersen, B. C., Bandura, K., et al. 2023, *ApJ*, 947, 83, doi: [10.3847/1538-4357/acc6c1](https://doi.org/10.3847/1538-4357/acc6c1)
- Chime/Frb Collaboration, Andersen, B. C., Bandura, K., Bhardwaj, M., et al. 2022, *Nature*, 607, 256, doi: [10.1038/s41586-022-04841-8](https://doi.org/10.1038/s41586-022-04841-8)
- Feng, Y., Li, D., Yang, Y.-P., et al. 2022, *Science*, 375, 1266, doi: [10.1126/science.abl7759](https://doi.org/10.1126/science.abl7759)
- Foreman-Mackey, D., Hogg, D. W., Lang, D., & Goodman, J. 2013, *PASP*, 125, 306, doi: [10.1086/670067](https://doi.org/10.1086/670067)
- Geyer, M., Serylak, M., Abbate, F., et al. 2021, *MNRAS*, 505, 4468, doi: [10.1093/mnras/stab1501](https://doi.org/10.1093/mnras/stab1501)
- Good, D., & Chime/Frb Collaboration. 2020, *The Astronomer's Telegram*, 14074, 1
- Harris, W. E., Harris, G. L. H., & Alessi, M. 2013, *ApJ*, 772, 82, doi: [10.1088/0004-637X/772/2/82](https://doi.org/10.1088/0004-637X/772/2/82)
- Jiang, P., Tang, N.-Y., Hou, L.-G., et al. 2020, *Research in Astronomy and Astrophysics*, 20, 064, doi: [10.1088/1674-4527/20/5/64](https://doi.org/10.1088/1674-4527/20/5/64)
- Keane, E. F. 2016, *MNRAS*, 459, 1360, doi: [10.1093/mnras/stw767](https://doi.org/10.1093/mnras/stw767)
- Kirsten, F., Snelders, M. P., Jenkins, M., et al. 2021, *Nature Astronomy*, 5, 414, doi: [10.1038/s41550-020-01246-3](https://doi.org/10.1038/s41550-020-01246-3)
- Kirsten, F., Marcote, B., Nimmo, K., et al. 2022, *Nature*, 602, 585, doi: [10.1038/s41586-021-04354-w](https://doi.org/10.1038/s41586-021-04354-w)
- Kirsten, F., Ould-Boukattine, O. S., Herrmann, W., et al. 2024, *Nature Astronomy*, 8, 337, doi: [10.1038/s41550-023-02153-z](https://doi.org/10.1038/s41550-023-02153-z)
- Kremer, K., Li, D., Lu, W., Piro, A. L., & Zhang, B. 2023, *ApJ*, 944, 6, doi: [10.3847/1538-4357/acabff](https://doi.org/10.3847/1538-4357/acabff)
- Kuzmin, A. D. 2007, *Ap&SS*, 308, 563, doi: [10.1007/s10509-007-9347-5](https://doi.org/10.1007/s10509-007-9347-5)
- Li, D., Wang, P., Zhu, W. W., et al. 2021, *Nature*, 598, 267, doi: [10.1038/s41586-021-03878-5](https://doi.org/10.1038/s41586-021-03878-5)
- Lorimer, D. R., Bailes, M., McLaughlin, M. A., Narkevic, D. J., & Crawford, F. 2007, *Science*, 318, 777, doi: [10.1126/science.1147532](https://doi.org/10.1126/science.1147532)
- Lorimer, D. R., & Kramer, M. 2004, *Handbook of Pulsar Astronomy*, Vol. 4
- Lu, W., Beniamini, P., & Kumar, P. 2022, *MNRAS*, 510, 1867, doi: [10.1093/mnras/stab3500](https://doi.org/10.1093/mnras/stab3500)
- Manchester, R. N., Hobbs, G. B., Teoh, A., & Hobbs, M. 2005, *AJ*, 129, 1993, doi: [10.1086/428488](https://doi.org/10.1086/428488)
- Nimmo, K., Hessels, J. W. T., Snelders, M. P., et al. 2023, *MNRAS*, 520, 2281, doi: [10.1093/mnras/stad269](https://doi.org/10.1093/mnras/stad269)
- Niu, C.-H., Li, D., Luo, R., et al. 2021, *ApJL*, 909, L8, doi: [10.3847/2041-8213/abe7f0](https://doi.org/10.3847/2041-8213/abe7f0)
- Niu, J. R., Wang, W. Y., Jiang, J. C., et al. 2024, *ApJL*, 972, L20, doi: [10.3847/2041-8213/ad7023](https://doi.org/10.3847/2041-8213/ad7023)
- Nyland, K., Young, L. M., Wrobel, J. M., et al. 2017, *MNRAS*, 464, 1029, doi: [10.1093/mnras/stw2385](https://doi.org/10.1093/mnras/stw2385)
- Oosterloo, T., Morganti, R., Crocker, A., et al. 2010, *MNRAS*, 409, 500, doi: [10.1111/j.1365-2966.2010.17351.x](https://doi.org/10.1111/j.1365-2966.2010.17351.x)
- Ould-Boukattine, O. S., Chawla, P., Hessels, J. W. T., et al. 2024, *arXiv e-prints*, arXiv:2410.17024, doi: [10.48550/arXiv.2410.17024](https://doi.org/10.48550/arXiv.2410.17024)
- Perley, R. A., & Butler, B. J. 2017, *ApJS*, 230, 7, doi: [10.3847/1538-4365/aa6df9](https://doi.org/10.3847/1538-4365/aa6df9)
- Pietka, M., Fender, R. P., & Keane, E. F. 2015, *MNRAS*, 446, 3687, doi: [10.1093/mnras/stu2335](https://doi.org/10.1093/mnras/stu2335)
- Snelders, M. P., Nimmo, K., Hessels, J. W. T., et al. 2023, *Nature Astronomy*, 7, 1486, doi: [10.1038/s41550-023-02101-x](https://doi.org/10.1038/s41550-023-02101-x)
- Spitler, L. G., Scholz, P., Hessels, J. W. T., et al. 2016, *Nature*, 531, 202, doi: [10.1038/nature17168](https://doi.org/10.1038/nature17168)
- Strader, J., Romanowsky, A. J., Brodie, J. P., et al. 2011, *ApJS*, 197, 33, doi: [10.1088/0067-0049/197/2/33](https://doi.org/10.1088/0067-0049/197/2/33)
- Suresh, A., Chatterjee, S., Cordes, J. M., & Crawford, F. 2021, *ApJ*, 920, 16, doi: [10.3847/1538-4357/ac1672](https://doi.org/10.3847/1538-4357/ac1672)
- Thornton, D., Stappers, B., Bailes, M., et al. 2013, *Science*, 341, 53, doi: [10.1126/science.1236789](https://doi.org/10.1126/science.1236789)
- Virtanen, P., Gommers, R., Oliphant, T. E., et al. 2020, *Nature Methods*, 17, 261, doi: [10.1038/s41592-019-0686-2](https://doi.org/10.1038/s41592-019-0686-2)
- Wang, W., Lu, J., Zhang, S., et al. 2019, *Science China Physics, Mechanics, and Astronomy*, 62, 979511, doi: [10.1007/s11433-018-9334-y](https://doi.org/10.1007/s11433-018-9334-y)
- White, R. L., & Becker, R. H. 1992, *ApJS*, 79, 331, doi: [10.1086/191656](https://doi.org/10.1086/191656)
- Xu, H., Niu, J. R., Chen, P., et al. 2022, *Nature*, 609, 685, doi: [10.1038/s41586-022-05071-8](https://doi.org/10.1038/s41586-022-05071-8)
- Zhang, B. 2018, *ApJL*, 867, L21, doi: [10.3847/2041-8213/aae8e3](https://doi.org/10.3847/2041-8213/aae8e3)
- . 2023, *Reviews of Modern Physics*, 95, 035005, doi: [10.1103/RevModPhys.95.035005](https://doi.org/10.1103/RevModPhys.95.035005)
- Zhang, S., & Yang, X. 2024, *ApJ*, 974, 248, doi: [10.3847/1538-4357/ad7857](https://doi.org/10.3847/1538-4357/ad7857)
- Zhang, S. B., Yang, X., Geng, J. J., Yang, Y. P., & Wu, X. F. 2024, *Detection of hidden emissions in two rotating radio transients with high surface magnetic fields*. <https://arxiv.org/abs/2407.09876>
- Zhang, S. B., Wang, J. S., Yang, X., et al. 2024a, *Nature Communications*, 15, 7454, doi: [10.1038/s41467-024-51711-0](https://doi.org/10.1038/s41467-024-51711-0)
- Zhang, S. B., Geng, J. J., Wang, J. S., et al. 2024b, *ApJ*, 972, 59, doi: [10.3847/1538-4357/ad6602](https://doi.org/10.3847/1538-4357/ad6602)
- Zhang, Y.-K., Li, D., Zhang, B., et al. 2023, *ApJ*, 955, 142, doi: [10.3847/1538-4357/aced0b](https://doi.org/10.3847/1538-4357/aced0b)
- Zhu, W., Xu, H., Zhou, D., et al. 2023, *Science Advances*, 9, eadf6198, doi: [10.1126/sciadv.adf6198](https://doi.org/10.1126/sciadv.adf6198)